



Immobilizing arsenic in contaminated anoxic aquifer sediment using sulfidated and uncoated zero-valent iron (ZVI)

Thiago Augusto Formentini^{a,*}, Geert Cornelis^a, Jon Petter Gustafsson^a, Kathrin Leicht^a, Charlotta Tiberg^b, Britta Planer-Friedrich^c, Neal Durant^d, Dimin Fan^d, Dan B. Kleja^a

^a Department of Soil and Environment, Swedish University of Agricultural Sciences, P. O. Box 7014, SE-750 07 Uppsala, Sweden

^b Swedish Geotechnical Institute (SGI), SE-581 93 Linköping, Sweden

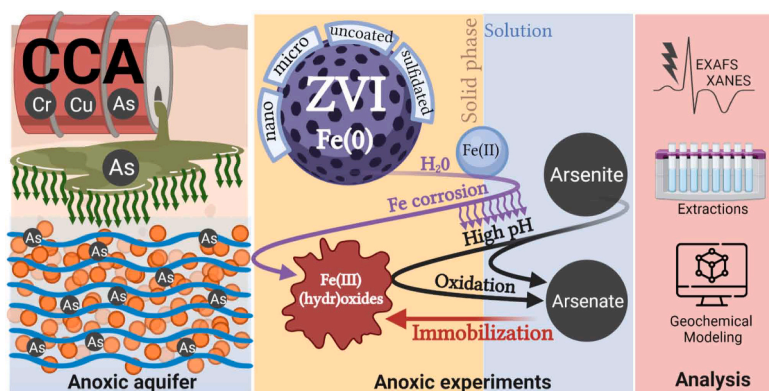
^c Environmental Geochemistry Group, Bayreuth Center for Ecology and Environmental Research (BAYCEER), Bayreuth University, 95440 Bayreuth, Germany

^d Geosyntec Consultants, Inc, 10211 Wincopin Circle, 4th Floor, Columbia, MD 21044, USA

HIGHLIGHTS

- Efficient immobilization of As at field-relevant conditions.
- Uncoated ZVI particles outcompeted sulfidated ZVI particles.
- Arsenite oxidation facilitated As sorption to ZVI corrosion products.
- Immobilization mechanisms in sediment suspensions differ from As spiked solutions.
- Role of ZVI coating, particle size, and corrosion products investigated and discussed.

GRAPHICAL ABSTRACT



ARTICLE INFO

Editor: <Feng Xiao>

Keywords:

Nanoparticles
Iron corrosion
Arsenic oxidation
Groundwater
Field conditions

ABSTRACT

Arsenic (As) is carcinogenic and of major concern in groundwater. We collected sediment material from a contaminated anoxic aquifer in Sweden and investigated the immobilization of As by four commercial zero-valent iron (ZVI) particles. Solid-phase As and Fe speciation was assessed using X-ray absorption spectroscopy (XAS) and solution-phase As speciation using chromatographic separation. Without ZVI addition, arsenite dominated in solution and As(V) species in the solid phase. Adding ZVI caused a sharp increase in solution pH (9.3–9.8), favoring As oxidation despite a lowered redox potential. ZVI greatly improved As retention by complex binding of arsenate to the Fe(III) (hydr)oxides formed by ZVI corrosion. Uncoated ZVI, both in nano- and microscale, performed better than their sulfidated counterparts, partly due to occlusion of As by the Fe(III) (hydr)oxides formed. The effect of particle size (micro vs. nano ZVI) on As immobilization was small, likely because immobilization was related to the corrosion products formed, rather than the initial size of the particles. Our results provide a strong geochemical background for the application of ZVI particles to remove As in

* Corresponding author.

E-mail address: thiago.formentini@slu.se (T.A. Formentini).

<https://doi.org/10.1016/j.jhazmat.2023.132743>

Received 27 June 2023; Received in revised form 31 August 2023; Accepted 7 October 2023

Available online 13 October 2023

0304-3894/© 2023 The Author(s). Published by Elsevier B.V. This is an open access article under the CC BY license (<http://creativecommons.org/licenses/by/4.0/>).

contaminated aquifers under anoxic conditions and illustrate that immobilization mechanisms can differ between ZVI in As spiked solutions and sediment suspensions.

Environmental implication: Arsenic ranks first on the list by the US ATSDR of substances posing a threat to human health and the WHO considers groundwater the riskiest source for human intake of As. However, dealing with As contamination remains a scientific challenge. We studied the immobilization of groundwater As by commercially available ZVI particles at field-realistic conditions. Arsenic immobilization was highly efficient in most cases, and the results suggest this is a promising in situ strategy with long-term performance. Our results provide a strong geochemical background for using ZVI to remove As in contaminated anoxic aquifers.

1. Introduction

Soil and groundwater contamination by arsenic (As) is widespread and endangers drinking water reserves in many parts of the world [35]. The sources of this contamination are in many cases geogenic, but can also be anthropogenic such as coal fly and bottom ash, mining, coal and petroleum extraction [3,43]. Soil As contamination from these sources occurs in various ways, e.g., atmospheric deposition, leaching or spill accidents [3]. Industrial use of chromated copper arsenate (CCA) is one of the major anthropogenic sources of As in soil and aquatic environments [29,31]. CCA has been utilized in the wood impregnation industry since the 1930s and became increasingly popular in the late 1980s [40]. Although restrictions have been imposed on the use of As in wood preservation since the early 2000s (e.g. European Commission Directive 2003/2/EC), the legacy of such sources still pose important threats to the environment [16,29,51]. Soil or groundwater As concentrations at CCA-impacted sites frequently exceed legal limit values, calling for urgent remediation actions. In-situ technologies are often preferred, especially if As has been spread to the saturated zone, where excavation will be expensive and technically challenging to perform.

Zero-valent iron (ZVI) has been deemed a suitable agent to treat a wide range of different contaminants, including As, because of its high reactivity [57]. ZVI can be used in permeable reactive barriers as granulated ZVI to prevent the spreading of contaminated groundwater plumes or injected as a slurry into aquifers making it useful to treat source zones in-situ [57]. ZVI can reduce redox-sensitive contaminants such as chlorinated hydrocarbons or chromate, rendering them less toxic and the reaction of ZVI with water produces different types of Fe oxides that can adsorb or co-precipitate with contaminants [32].

The most relevant As redox states in groundwater are As(V) and As(III), where As(III) species are more toxic, more mobile, and usually dominate in anoxic aquifers. Species of both redox states can react in various ways with ZVI. As(V) can be (i) reduced to As(III) by ZVI or even to the sparingly soluble As(0) and/or (ii) adsorbed to or coprecipitate with different types of iron oxides formed from oxidized ZVI [37,58]. ZVI has also shown great promise for immobilizing As(III) species under anoxic conditions in controlled laboratory experiments. In water suspensions, ZVI can have dual redox functions on As(III), i.e. As(III) can either be reduced to As(0) by the metallic core or oxidized to As(V) by the Fe (hydr)oxide layer formed upon oxidation of the metallic core [37]. The “reductive power” of ZVI seems to be related to both particle size and surface properties of the particles. Several studies using nano-sized ZVI (nZVI) materials have confirmed the ability of the Fe(0) core to reduce As(III) to insoluble As(0) and/or an intermetallic phase with the Fe(0) core [28,37,58,67]. According to Tuček et al. [58], the reduction of As(III) to As(0) might be impeded by the iron (hydr)oxide shell formed on particle surfaces in contact with water. Immobilization of As(III) species by micro-sized ZVI (mZVI) seems to occur via sorption of As(V) and As(III) species by the iron (hydr)oxide layer [53,23]. The extent to which these immobilization reactions occur also depends on various parameters such as pH, Eh and the presence of competing anions such as phosphate [28,32]. While published literature provides multiple examples involving treatment of aqueous solutions spiked with As(III) or As(V), the potential of mZVI and nZVI materials to immobilize As(III) at anoxic conditions has hitherto not been tested thoroughly with actual

soil or sediment materials or in the field.

Using partially sulfidated ZVI is a relatively new approach that has shown a great potential to improve the efficiency of ZVI for soil remediation during controlled laboratory experiments. The presence of an FeS coating suppresses the reaction of Fe(0) with water and increases the dechlorination potential of nZVI [10]. The presence of sulfide also extends the application of ZVI beyond contaminants that can be reduced (e.g. Cr(VI)) to also remediate metals that have a low sulfide solubility (e.g. Cd, Zn). For As, sulfidation of nZVI has recently been shown to enhance removal capacity and rate compared to uncoated ZVI, which was attributed to a thicker surface layer and formation of arsenite inner-sphere complexes [66]. The presence of sulfide can also lead to (i) the formation of aqueous monothioarsenate from arsenite and zero-valent sulfur species or (ii) the formation of aqueous higher thio-lated arsenates at higher free sulfide ratios [4]. The Formation of thioarsenates makes predicting removal capacity and rate more complicated. While mono- and trithioarsenate sorb less than arsenite and arsenate to goethite or mackinawite, only trithioarsenate also sorbs weakly to pyrite, whereas monothioarsenate showed a 100% removal with pyrite [8]. For ZVI, monothioarsenate removal rate was reported to be only slightly less than that of arsenate and substantially higher than that of arsenite [34].

In this work, we investigated the binding mechanisms and extent of immobilization of As by four commercially available ZVI reagents at anoxic conditions. Both sulfidated and non-sulfidated nZVI and mZVI were investigated, due to their potentially different binding mechanism (s) for As. Immobilization of As species by nano- and micro sized ZVI at realistic conditions using actual soil or sediment materials has been scarcely studied under anoxic conditions. Moreover, a thorough comparison of As treatment performance taking into account ZVI particle size and surface coating, i.e. mZVI, S-mZVI, nZVI, and S-nZVI, is lacking. We therefore sampled sediment material from an anoxic aquifer historically contaminated by a CCA spill where dissolved As occurs predominantly as arsenite. nZVI is hypothesized to be more mobile in aquifers, when stabilized with organic polymer, and more reactive because of its high specific surface area, compared to micro-sized ZVI [57]. Conversely, mZVI is cheaper, but has a lower surface area and reactivity as a reductant and/or lower production of iron (hydr)oxides, which lends it a longer lifetime compared to nZVI [57]. Immobilization of As by the different ZVI materials was investigated as a function of time in batch experiments using contaminated sediments. To assess reaction mechanisms, analytical speciation of dissolved As was made using chromatographic separation, whereas solid-phase As and Fe were characterized using a combination of X-ray absorption spectroscopy (XAS) and extraction methods. A thorough mechanistic understanding of immobilization mechanisms is crucial for a reliable assessment of the ability of different ZVI formulations to immobilize As in the field and how robust this immobilization will be in a long-term perspective.

2. Materials and methods

2.1. Study area and sampling

The contaminated aquifer is situated at 57°37'36"N, 15°20'54"E in Hjaltevad, Eksjö municipality, southern Sweden. It covers 5.3 ha and is

168 m above mean sea level. The soil consists mainly of glaciofluvial deposits that were gradually built up in layers of sand, gravel and silt. A wood impregnation plant using water-based wood preservatives, particularly CCA, was operated from 1949 to 1985. In 1968, leakage from a steel tank containing 50 m³ of CCA located 0.5–1.0 m below the surface was detected. An estimated amount of 65–80 kg As, as arsenate, leaked to the groundwater. A detailed site description is presented by Cao et al. [7].

A contaminated sediment sample was collected using sonic drilling in the source zone. A core sample was taken 16–18 m below the surface, corresponding to 7–9 m below the groundwater surface. Anoxic conditions during sampling were maintained by bubbling N₂ gas through the sample when transferring it from the Aqualock core sampler to a Plexiglas tube. The Plexiglas tube was immediately sealed with rubber stoppers and transferred to a freezer. The frozen core was later thawed in a glovebox (Section 2.3), homogenized and transferred to Mylar® bags in portions. The sealed Mylar® bags were stored in a freezer (−18 °C) until usage in the experiments.

2.2. ZVI particles

Sulfidated mZVI (S-mZVI), commercially available as S-MicroZVI® (Regenesis) is a viscous, dark grey, colloidal suspension containing 40 % Fe(0) and 1–2 % Fe(II) sulfide by weight (S/Fe mass ratio of 0.009–0.018) suspended in glycerol, consisting of spherical-shaped particles with 2–3 μm diameter. mZVI, commercially available as Ferox Target® (Hepure Technologies), is a black powder containing 95 % Fe(0), 1.5–2.0 % C, 1.0–1.5 % Si, 0.1 % S and P, and a nominal particle diameter of 44 μm. S-nZVI, commercially available as NANOIRON 25DS® (NANOIRON) is an aqueous suspension containing 14–18 % Fe(0), 2–6 % Fe(II) oxide by weight, with inorganic sulfur-based structures on the surface leading to a S/Fe mass ratio of 0.01 (1 %). nZVI, commercially available as NANOIRON 25® (NANOIRON) is analogous to its sulfidated counterpart, but has no sulfur-based structures on the surface. The nominal particle diameter for both S-nZVI and nZVI is 50 nm, though aggregation has been reported in both cases [41,5,6]. In addition, S-nZVI material having a S/Fe mass ratio of 0.2 was produced as test material by NANOIRON to investigate whether a higher S/Fe ratio could contribute to additional As(III) immobilization.

2.3. Batch experiments

The batch experiments were conducted at anoxic conditions in a N₂-saturated glovebox (Labconco, USA) equipped with catalytic O₂ removal. Artificial groundwater (AGW) with ionic composition matching the As-contaminated aquifer was prepared using degassed ultra-pure water (ELGA, USA) spiked with 0.015 mM NH₄⁺, 0.45 mM Ca²⁺, 0.1 mM Mg²⁺, 0.01 mM Mn²⁺, 0.75 mM Na⁺, 0.05 mM K⁺, 1.14 mM Cl⁻, 0.2 mM SO₄²⁻, 0.001 mM PO₄³⁻, and 0.8 mM HCO₃⁻ using CaCl₂, NaHCO₃, KHCO₃, MgCl₂, MnCl₂, NH₄Cl, KH₂PO₄, and K₂SO₄ salts. To match the site groundwater, the final pH of the AGW was adjusted to 6.0 using diluted HCl.

Eighteen grams of As-contaminated aquifer sediment (13 % water content) were mixed with 90 mL of AGW in a 100-mL polypropylene tube (liquid-to-solid ratio = 5.9). Viscous S-mZVI and powder mZVI were dosed by mass, while aqueous S-nZVI and nZVI suspensions were dosed by volume, and then added to the mixture of AGW and sediment. Control microcosms were also prepared, without ZVI addition. The target ZVI-to-sediment dose was 0.2 wt% for S-mZVI, S-nZVI and nZVI, and 1 wt% for mZVI. A higher mZVI dose was seen as relevant since mZVI will in practice be used at higher doses than the other three ZVI materials, because the mass-based cost and specific surface area of mZVI are lower. In addition, mZVI is expected to be less mobile than S-mZVI and less reactive than nZVI. The amount of Fe added to soils via ZVI products was confirmed by digesting the stocks using *aqua regia* (Section 2.5). The measured ZVI additions were 0.23 wt% for S-mZVI (0.39 g Fe/

L), 0.33 wt% for S-nZVI (0.56 g Fe/L), 0.31 wt% for nZVI (0.53 g Fe/L), and 1.1 wt% for mZVI (1.86 g Fe/L). Sixteen 100-mL soil-ZVI suspensions were prepared for each ZVI product and the control. The tubes were shaken simultaneously in end-over-end shakers and removed individually for analysis after given times.

Firstly, the experiment was carried out without pH adjustment over a maximum of 30 days (deemed sufficient for reaching steady-state conditions in preliminary experiments), with individual tubes sampled every 3–5 days. This period with no pH adjustment is hereafter denoted phase A. Secondly, the pH was adjusted to 7 to simulate a long-term situation where the system pH returns to values equivalent to before ZVI addition (i.e. the pH of the control without ZVI addition), thus allowing investigation of the individual effect of pH on As immobilization by ZVI. Although pH buffers were used previously to study As sorption/precipitation (e.g. [65,19,62]), they may introduce artifacts [21] affecting ZVI reactivity with As. Hence, pH buffers were avoided in this study. Instead, pH was adjusted using diluted HCl in six tubes per ZVI material that had previously equilibrated for 33 days. These tubes were put back into the shaker and finally sampled in duplicate at additional shaking times of 7, 14, and 35 days, together with six control tubes. This period with adjusted pH is hereafter denoted phase B. Sampling times for each ZVI microcosm during phases A and B are summarized in the Supporting Information (Table S1). Since S-mZVI addition little affected solution pH (Section 3.1.3), this material was investigated only in phase A.

After removal from the shaker, capped and sealed tubes were removed from the glovebox and centrifuged for 15 min at 1450 relative centrifugal force (g) (Allegra X15R). Following centrifugation, the tubes were immediately transferred back to the glovebox for measurement of pH and redox potential (Eh) of the unfiltered supernatants (Orion ROSS Ultra and Sure Flow, Thermo Scientific, USA). The uncertainty of the Eh measurements was ± 60 mV according to the manufacturer. The remaining supernatant was filtered through 0.45-μm PES syringe filters (S-mZVI and mZVI) or 0.1-μm PES syringe filters (S-nZVI and nZVI).

A 15-mL portion of the filtered supernatant was preserved with 1 % HNO₃ for analysis of total As and Fe concentrations. Another 15-mL portion of the filtered supernatant was passed through an As speciation cartridge (MetalSoft Center) containing aluminosilicate sorbent selectively retaining the negatively charged arsenate (and potentially present thioarsenate anions) and letting the non-charged arsenite pass the cartridge [24]. The cartridge filtrate was preserved with 1 % HNO₃ for analysis of As concentration. The amount of As retained by the cartridge was estimated based on the difference between total As and the As concentration passing the cartridge. A 1.8-mL portion of the filtered supernatant was spiked with 0.18 mL of 10 mM HBED (hydroxybenzyl ethylenediamine, an Fe chelating agent) in a 2-mL cryogenic vial and immediately flash-frozen by immersion in a liquid nitrogen bath (−196 °C) for separation of arsenite, arsenate, and inorganic thioarsenates in selected samples via ion chromatography (Section 2.4; [63]). The ion chromatography method indicated that arsenite concentrations were in good agreement with the As concentrations in solutions passing the speciation cartridges (Table S2).

The remaining filtered supernatant was preserved at −20 °C for analysis of P-PO₄, Cl, SO₄, and TOC. All sample preparation was performed in the glovebox. The solid fraction that settled during centrifugation was flash-frozen in liquid nitrogen (−196 °C) and freeze-dried at −47 °C for analyses of total and extractable As and Fe contents and for synchrotron-based X-ray absorption spectroscopy (XAS) analysis. Freeze-dried samples were stored and transported in sealed Mylar® bags to minimize contact with oxygen prior to the analyses with XAS (Section 2.5).

2.4. Solution analyses

Samples for total concentrations of As and Fe as well as the eluted samples from the As speciation cartridge were analyzed using sector

field inductively coupled plasma mass spectrometry (ICP-SFMS) according to SIS [48] and U.S. EPA [59]. From the HBED-stabilized, flash-frozen samples, arsenite, arsenate, and inorganic thioarsenates were determined using ion chromatography (IC, ICS-3000, Dionex, USA) coupled to inductively coupled plasma-mass spectrometry (ICP-MS, XSeries II, Thermo-Fisher, USA) as in Wang et al. [63]. Sulfate (SO₄) and chloride (Cl) in solution were analyzed using ion chromatography (IC, 930 Compact IC Flex, Metrohm, Switzerland) according to SIS [47]. TOC in solution was analyzed using a total organic carbon analyzer (TOC-VCPH, Shimadzu, Japan) according to SIS [46]. PO₄ in solution was analyzed using a segmented flow analyzer (SFA, QuAAtro, Seal Analytical, UK) according to SIS [49].

2.5. Solid-phase analyses

Solid-phase analyses were performed on centrifuged, flash-frozen, freeze-dried sediment samples isolated from the solution at the end of phase A (23 or 30 days equilibration). In addition, the contaminated sediment used for the laboratory experiments was analyzed before equilibration with AGW or ZVI addition, hereafter denoted the untreated contaminated sediment. Mineralogical and key chemical characteristics of the untreated contaminated sediment are summarized in Fig. S1 and Tables S3 and S4. Solid-phase As and Fe concentrations were determined after 0.5 g dried sediment and *aqua regia* (1.25 mL of 65 % HNO₃ and 3.75 mL of 37 % HCl) were added to 80 mL PTFE vessels and subjected to microwave-assisted digestion (Ethos Easy, Milestone, Italy) [17]. Digests were filtered, diluted to 50 mL with ultrapure water and analyzed using inductively coupled optical emission spectroscopy (ICP-OES).

An estimate of As and Fe associated with amorphous iron (hydr) oxide precipitates was obtained using oxalate extraction according to van Reeuwijk [60]. 50 mL of 0.2 M oxalate solution (pH 3) was added to 0.50 g of freeze-dried sample. The suspensions were shaken for 4 h in the dark on an end-over-end shaker and then centrifuged at 3725 g for 15 min. The supernatants were filtered through 0.2- μ m PES syringe filters (Sarstedt®, polyethersulfone membrane) and As and Fe were quantified in the filtrate using ICP-MS.

In addition, treated and untreated sediment materials were extracted with phosphate solution to estimate the concentration of accessible, surface-bound As [64,66]. 0.5 g of freeze-dried sample was mixed with 50 mL of 0.5 M phosphate solution (pH 8) in a 50-mL centrifuge tube. The suspension was shaken for 16 h on an end-over-end shaker and then centrifuged at 3725 g for 15 min. The supernatant was filtered through a 0.2- μ m PES syringe filter. The phosphate extracts were preserved until analysis by acidifying to 4 % HNO₃. As and Fe in the extracts were analyzed using ICP-MS.

Solid-phase speciation of As and Fe in reacted sediment samples was obtained using As and Fe K-edge XAS performed at the Balder beamline at the MAX IV laboratory, Lund, Sweden. The beamline was equipped with a Si[111] double crystal monochromator. Finely ground samples were spread and pressed on sample holders and analyzed at liquid He temperature (15 K) to prevent sample damage by photoreduction and to increase the signal-to-noise ratio. The signal was acquired in fluorescence mode using a seven-element Ge detector. When collecting As fluorescence data, a Cu 3 λ -filter and an Al foil were used. For As, internal energy calibration was performed using the L₃ edge energy of Au foil set at 11.919 keV. For Fe, Fe foil was used, with E₀ set to the Fe K edge at 7.112 keV [56]. Sixteen scans were collected for each sample. Merging, normalization, and first-shell fitting were performed according to standard methods [18] using the Demeter software suite [38].

For performing As K-edge extended X-ray absorption fine structure analysis (EXAFS), the background was removed using the AUTOBAK algorithm in Athena, with a *k*-weight of 3 and with the Rbkg parameter set to 0.85. The scans were then imported to Artemis [38] for final treatment of the EXAFS spectra, producing a model for the first-shell contributions. Theoretical phase and amplitude functions for single

and multiple scattering (MS) paths were calculated using the FEFF software package [39], using the structure of scorodite [20]. Multiple scattering within the AsO₄ tetrahedron was accounted for by a three-legged triangular As–O–O MS path (CN = 12), with its path length (R) set to 1.8165 times the path length of the first-shell As–O path, and its Debye-Waller factor assumed to be equal to that of the As–O path. Fourier transforms (FT) were calculated using a Hanning window between appropriate *k*-ranges, as mentioned in the Results section. Using Artemis, the FT data were fitted between 0.85 and 3.5 Å in *k*-weights 1, 2, and 3 simultaneously.

For Fe K-edge EXAFS, the same procedures were used, except that the Rbkg parameter was set to 1, the model was derived using the Fe–O coordination in ferrihydrite [25], and the FT data were fitted between 1 and 2 Å. In this case, MS contributions were not considered. Moreover, each normalized sample spectrum was subjected to linear combination fitting (LCF) analysis in the X-ray near edge structure (XANES) region between 7.102 and 7.162 keV. The LCF-LinEst code was used, which relies on the Microsoft Excel LinEst function for optimization [1,13]. In the LCF, energy shifts were not permitted, the sum of weights (SOW) was not forced to 1, and a maximum of four standards was allowed in the output. Outputs resulting in SOW < 0.95 and > 1.05 were not accepted. The best fit was chosen using the normalized residual sum-of-squares (NRSS) as the goodness-of-fit parameter:

$$\text{NRSS} = \frac{\sum_i [(data_i - fit_i)^2]}{\sum_i data_i^2} \quad (1)$$

Further, to determine the uncertainty of the obtained LCF weights, uncertainty analysis (as described by [14]) was performed using LCF-LinEst, with the Beta distribution α and β parameters set to 1.5, the energy calibration error set to 0.2 eV, the maximum relative normalization error set to 10%, and by using the Latin Hypercube method to sample 100 spectra. The standards used in the analysis were Fe(0) foil, Fe(III) complexed to fulvic acid (FeFA; [61]), biotite [55], ferrihydrite and goethite [30]. While Fe(0) foil was assumed to represent unreacted ZVI, FeFA represented organically complexed Fe(III), and biotite was used as a proxy for Fe(II)-containing silicate minerals such as trioctahedral mica [36].

2.6. Geochemical modeling

Thermodynamic data for equilibrium calculations made for soluble As are given in Supporting Information (Table S5). In addition, a quantitative estimate of the amount of As bound by a hypothetical ferrihydrite phase (HFO) under relevant experimental conditions was obtained using the software Visual MINTEQ [12]. The model accounts for pH and redox-dependent reactions of As in the aqueous phase as well as in the adsorbed phase. The input data and procedure used in the modelling is given in Supporting Information (Table S6). The model was used to calculate the Eh values at which 50% of adsorbed As was arsenite and 50% arsenate at pH values 6.0, 7.0, 8.0 and 9.0 (Table S7). Calculations were made for two different HFO concentrations to assess possible variation owing to HFO concentrations.

3. Results

3.1. Solution phase

3.1.1. Control: no ZVI addition

Fig. 1 shows the temporal dynamics of total As and Fe, arsenite and Fe(II), pH and Eh in the solution phase of control sediment suspensions with no added ZVI. Initially (*t* < 10 d), arsenite accounted for a low proportion of total As in solution. After 10 d, the As speciation became dominated by arsenite and total As increased substantially. The system stabilized at a total As concentration of ca. 1200 μ g/L after 30 d, with a

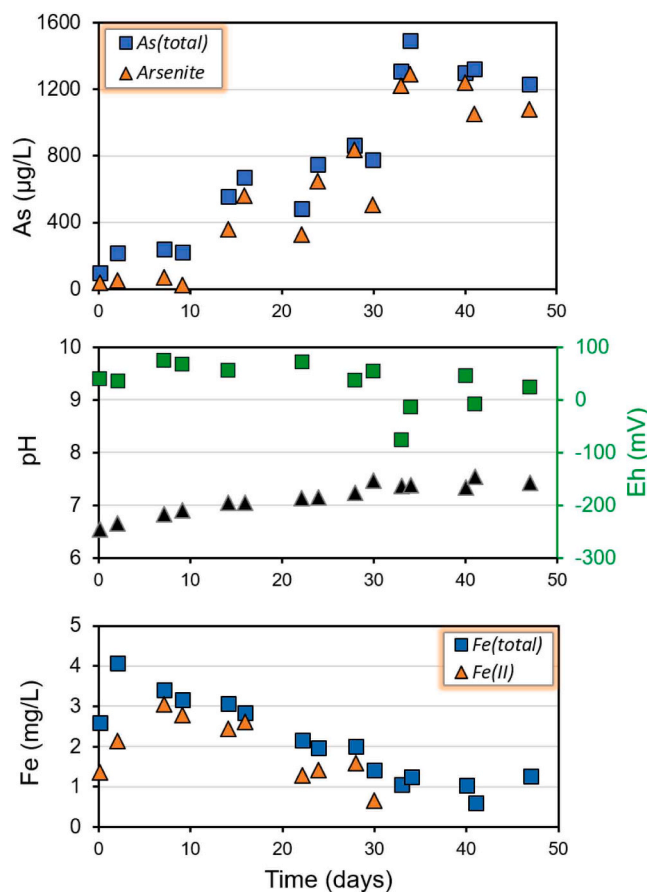


Fig. 1. Temporal dynamics of solution-phase As, Fe, pH, and Eh within anoxic control microcosms containing artificial groundwater (AGW) and As-contaminated aquifer sediment. AGW had pH 6 and was As- and Fe-free before mixing.

median solution-phase arsenite/As(total) ratio of 0.88 ($t = 33\text{--}47$ d). There was a slight drift in pH during equilibration, from 6.5 to 7.3, whereas Eh remained fairly constant, fluctuating around 0 mV. The predominance of arsenite in solution was mirrored by the predominance of Fe(II) in solution (Fig. 1, bottom), reflecting the similar redox properties of the As(V)/As(III) and Fe(III)/Fe(II) redox couples. The conditions obtained in the laboratory were consistent with field measurements of groundwater chemistry made close (<20 m) to the sampled sediment core, where the average total As concentration was $889\ \mu\text{g/L}$, arsenite dominated As speciation and the average pH and Eh were 6.2 and -26 mV, respectively (Table S8). These conditions are also in line with many other anoxic groundwaters around the world [52].

3.1.2. mZVI and nZVI treated sediment

mZVI and nZVI addition to the groundwater-sediment system increased the solution pH to 9.4–9.8 and decreased the Eh to below -200 mV at the end of phase A (Fig. 2). The pH rise indicates anaerobic corrosion of the Fe(0) core according to Reaction 1 [44]:



Due to the high pH, dissolved $\text{Fe}^{2+}/\text{Fe}^{3+}$ released to solution was rapidly hydrolyzed and precipitated as Fe (hydr)oxides (Section 3.2), in agreement with the low concentration of dissolved Fe during phase A (Fig. 2, bottom). Dissolved As was only $11\ \mu\text{g/L}$ using mZVI ($t = 30$ d) and $19\ \mu\text{g/L}$ using nZVI ($t = 23$ d), which represents $\leq 3\%$ of the dissolved As detected in the control where no ZVI was added (Fig. 1). The residual solution-phase As during phase A (uncontrolled pH) was dominated by arsenate with a median arsenite/As(total) ratio of 0.18

(mZVI) and 0.09 (nZVI). In phase B ($t > 33$ d), the pH was adjusted to 7 to assess the behavior of previously immobilized As at circumneutral pH, a long-term condition expected in the field when the rate of Fe(0) corrosion slows down due to surface passivation. In both mZVI and nZVI systems, dissolved As concentrations remained low, representing $< 1\%$ of the control in the mZVI system and 5% of the control in the nZVI system at the final measurement ($t = 68$ d). Despite the lower pH in phase B, residual solution-phase As still contained a low arsenite concentration compared to the control experiment, with the median arsenite/As(total) ratio at 0.28 (mZVI) or 0.17 (nZVI).

The pH adjustment to 7 in the sediment-ZVI suspensions (phase B) resulted in a substantial release of Fe, as high as $659\ \text{mg/L}$ and $138\ \text{mg/L}$ in the mZVI and nZVI systems, respectively (Fig. 2, bottom). This corresponded to ca. $1/3$ of the total Fe added via ZVI in each case, suggesting that part of the Fe (hydr)oxides formed from corrosion during phase A (uncontrolled pH) might have undergone reductive dissolution at pH 7 in phase B, as illustrated by dissolution of $\text{Fe}(\text{OH})_{3(s)}$ below.



3.1.3. S-mZVI and S-nZVI treated sediment

S-mZVI addition did not increase the solution pH in comparison to the control groundwater-sediment system, remaining at ca. 7.3 throughout the 30 days experimental time (Fig. 3). The Eh, however, slightly decreased to approximately -100 mV. According to the manufacturer, the commercial S-mZVI is dispersed in 40% glycerol and some additives, which explains the higher DOC concentration ($150\ \text{mg/L}$) in the S-mZVI treated systems (Fig. S4). However, due to the very weak acid properties of glycerol ($\text{pK}_a = 14.4$; [42]), its presence could not contribute to buffer the pH. Instead, the minor effect on pH by these particles is probably explained by the FeS alteration, which slowed down the corrosion rate, as indicated by XAS analysis (Section 3.2).

Dissolved total As decreased gradually from $111\ \mu\text{g/L}$ initially to $29\ \mu\text{g/L}$ after 30 d. The latter value corresponds to 4% of the dissolved As in the control system with no ZVI addition. The median solution-phase arsenite/As(total) ratio during equilibration with S-mZVI was only 0.11. Moreover, the concentration of monothioarsenate had a maximum of $2.2\ \mu\text{g/L}$ at $t = 16$ d. Indeed, most of the residual dissolved As in the S-mZVI system was arsenate (Fig. 3, Table S2). Unlike the other ZVI particles tested, the dissolved Fe concentration using S-mZVI was high after 10 d of equilibration ($>20\ \text{mg/L}$) and consisted mostly of Fe (II) (Fig. 3). This is likely due to the relatively lower pH in the S-mZVI treatment (ca. 7.3), causing higher Fe(II) formation and less formation of Fe(III) (hydr)oxide corrosion products.

S-nZVI affected pH and Eh in a similar way as its uncoated counterpart, i.e. pH increased to ~ 9.3 and Eh decreased to approximately -200 mV (Fig. 3). This suggests that anaerobic corrosion of the Fe(0) core took place according to Reaction 1. In contrast to treatment with uncoated nZVI, soluble As concentrations remained relatively high throughout the 23-days reaction time, i.e. $>100\ \mu\text{g/L}$ or about 15% of the soluble As present in the control with no ZVI addition. Arsenite made up less than 5% of the residual As concentration in solution, and the monothioarsenate concentration was at $15\ \mu\text{g/L}$ at the end of phase A (Fig. 3, Table S2). Accordingly, residual As in solution was strongly dominated by arsenate.

Following adjustment to pH 7 (phase B), the S-nZVI system behaved similarly as the uncoated nZVI system with respect to Eh and dissolved Fe (Fig. 3). Although Fe concentrations corresponding to about $1/3$ of the added S-nZVI were released to solution, solution-phase As decreased after pH adjustment, reaching $47\ \mu\text{g/L}$ at $t = 68$ d. Similar to phase A, dissolved As in phase B contained low arsenite proportion, with median arsenite/As(total) of 0.15.

To assess the effect of degree of sulfidation of nZVI particles on As retention, S-nZVI material with a S/Fe mass ratio of 0.2 was also tested.

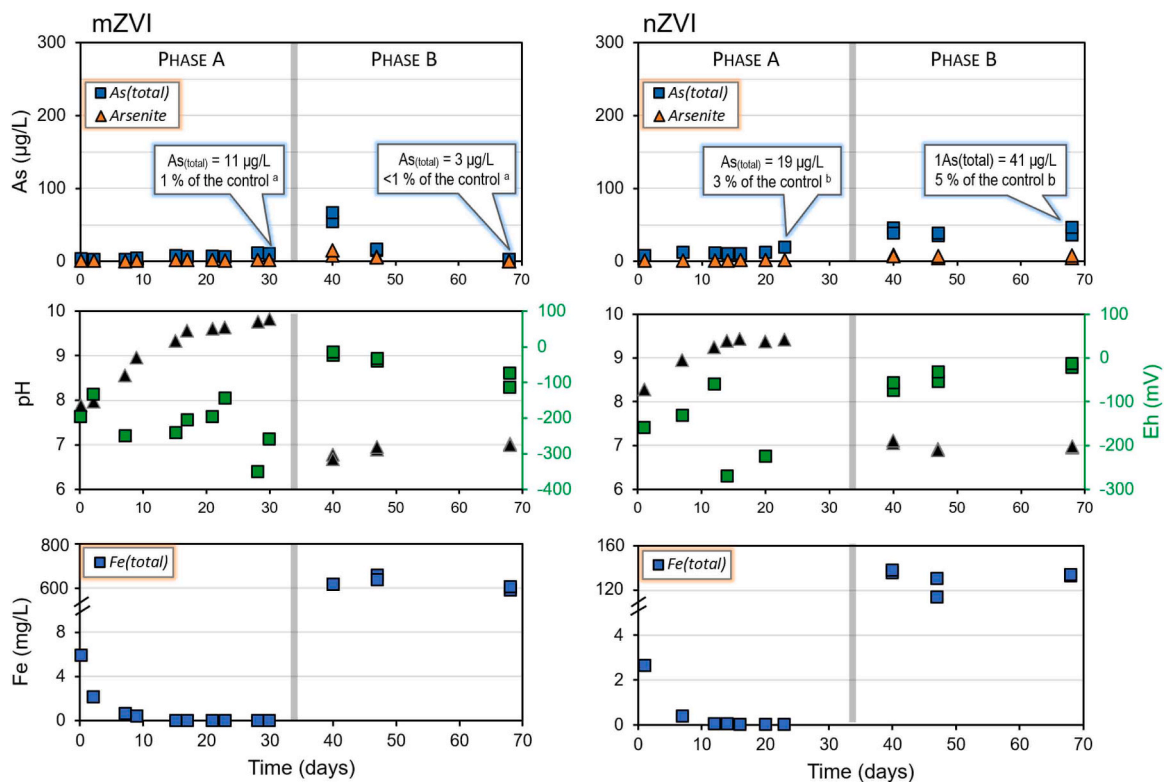


Fig. 2. Temporal dynamics of solution-phase As, Fe, pH, and Eh within anoxic microcosms containing artificial groundwater (AGW), As-contaminated aquifer sediment and (left) mZVI or (right) nZVI. AGW had pH 6 and was As- and Fe-free before mixing. Phase A: uncontrolled pH. Phase B: pH adjusted to 7. (^a Compared to the control at $t = 30$ d; ^b compared to the control at $t = 23$ d).

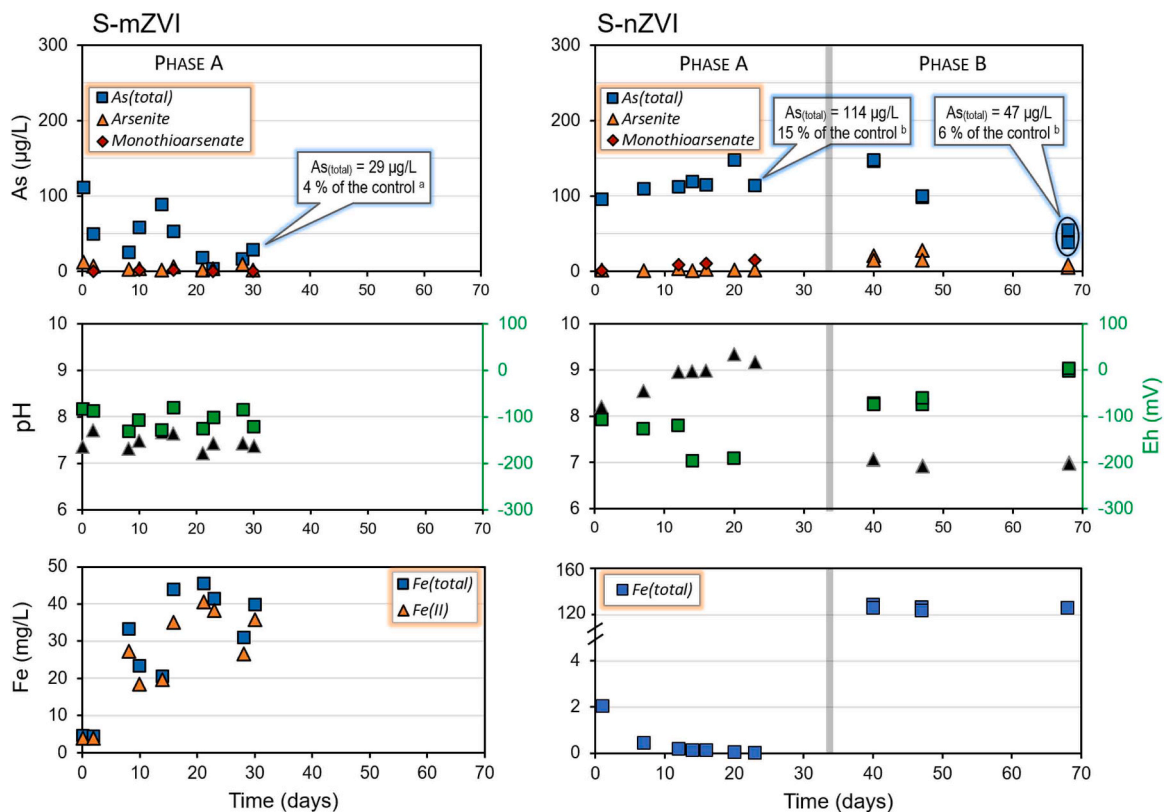


Fig. 3. Temporal dynamics of solution-phase As, Fe, pH, and Eh within anoxic microcosms containing artificial groundwater (AGW), As-contaminated aquifer sediment and (left) S-mZVI or (right) S-nZVI. AGW had pH 6 and was As- and Fe-free before mixing. Phase A: uncontrolled pH. Phase B: pH adjusted to 7. (^a Compared to the control at $t = 30$ d; ^b compared to the control at $t = 23$ d).

These particles showed no detectable As retention capacity and even promoted dissolution of sorbed As in comparison to the control system with no ZVI added (Fig. S2). After 10 d equilibration, concentrations of dissolved As higher than 2000 µg/L were observed, dominated by arsenate (Table S2). Mobilization of As was probably due to the very high pH (~10.5) caused by these particles, which promoted desorption of arsenate bound to indigenous Fe/Al (hydr)oxides [50,7]. According to the manufacturer, the high pH was likely due to excess of unreacted, “free” sulfide caused by the high degree of sulfidation.

3.2. Solid phase speciation of Fe

The ratio between the ZVI dosed for injection (Section 2.3) and the measured total Fe concentration after *aqua regia* digestion in all ZVI treatments ranged between 0.81 and 1.03 (Table 1). In the untreated contaminated sediment used for the experiments, the oxalate-extractable Fe concentration was 0.69 g/kg of dry sediment, representing 9 % of the total Fe concentration, and also similar to the control sample after 30 days equilibration with AGW (0.65 g/kg). Oxalate-extractable concentrations of Fe increased considerably in samples treated with ZVIs, representing 25–52 % of the total Fe in these systems. This indicates that a significant part of the added ZVI was transformed to amorphous Fe (hydr)oxides [33] during phase A (uncontrolled pH). Moreover, the dissolution of ca. 1/3 of added ZVI (Figs. 2 and 3) for the three ZVIs (mZVI, nZVI and S-nZVI) tested in phase B (pH 7) indicates a high reactivity of the corrosion products formed, which is not expected for e.g. mineral Fe (hydr)oxides.

The Fe K-edge XANES spectra for the control, ZVI-treated samples, and selected reference compounds are shown in Fig. 4. The energy position of the white line (sharp rise in absorption) was intermediate to those of biotite and ferrihydrite, implying that the samples contained both Fe(II) and Fe(III), resulting from the presence of Fe(II)-containing silicate minerals and Fe(III) (hydr)oxides such as ferrihydrite and goethite. The presence of trioctahedral micas like biotite in the untreated contaminated sample was confirmed with X-ray diffraction analysis (Fig. S1). The spectra for sediment samples treated with mZVI and S-mZVI showed considerable enhancement in the region around the edge of Fe(0), suggesting a portion of unreacted Fe(0) remained. This is in agreement with LCF results (Table 2, Fig. S3), which also indicated a minor additional contribution of organically complexed Fe(III), particularly in the control sample.

Combining the LCF-based percent speciation for the sediment-ZVI systems (Table 2) with the amount of Fe(0) added in each treatment (Table 1), 4 % of the nZVI, 16 % of the S-nZVI, 36 % of the mZVI, and 91 % of the S-mZVI remained as Fe(0) at the end of phase A. For the S-mZVI treated sample, this is somewhat inconsistent with the oxalate extraction data that indicated a significant corrosion of the Fe(0) core. However,

EXAFS analysis (Fig. 4, Table S10) further supported the presence of a considerable fraction of residual Fe(0) in this sample as well as in the sediment sample treated with mZVI, which manifested itself at 5.1, 6.6 and 8 Å⁻¹ (vertical dashed lines in Fig. 4). Moreover, the EXAFS model fittings of the first shell are consistent with a predominance of Fe–O paths with path lengths ranging from 2.02 to 2.07 Å (Table S9), intermediate to the Fe–O distances expected for ferrihydrite (1.97–1.99 Å; [26]) and aqueous Fe²⁺ (~2.1 Å; [9]), again indicating that all the samples contained Fe(II)-containing silicates and Fe(III) in poorly ordered (hydr)oxides.

3.3. Solid phase speciation of As

The concentration of oxalate-extractable As in the untreated contaminated sediment used for the laboratory experiments (37.6 mg/kg of dry sediment, Table 1) indicated that about 70 % of the total As concentration (53.9 mg/kg) was associated with amorphous Fe (hydr)oxides. In the control sample (sediment mixed with groundwater but no ZVI addition), 10 % of total As (dissolved + *aqua regia*-digested As) was dissolved (4.6 mg/kg), whereas only about 1 % or less of total As was dissolved in the ZVI-treated samples (0.06–0.67 mg/kg) at the end of phase A. In addition, phosphate-extractable As concentrations in the mZVI and nZVI treatments were also lower than in the control treatment (Table 1). Assuming that phosphate competes with adsorbed As [64,66], this observation suggests that some As bound by mZVI and nZVI corrosion products was occluded and thereby less available for exchange with phosphate.

The As K-edge XANES spectra for the control and ZVI-treated samples at the end of phase A are shown in Fig. 5, together with selected As reference compounds. Spectra of control and ZVI-treated samples are very similar and show an absorption edge energy consistent with As(V) surrounded by O atoms in the first coordination shell. This is in agreement with EXAFS fitting of the first shell revealing As–O path distances at around 1.70 Å (Table S10), consistent with As(V) in an AsO₄ tetrahedron. Both the fitted EXAFS parameters and the general appearance of the spectra were in close agreement with what would be expected for adsorbed AsO₄ tetrahedra on common soil minerals such as ferrihydrite and Al(OH)_{3(s)} (Fig. 5). However, they are dissimilar to those expected for a Fe-AsO₄ phase such as scorodite [27], as this would lead to larger spectral distortion due to stronger second-shell As···Fe contributions. Also, the involvement of any S in the first shell (such as in As(V) sulfide or in monothioarsenate) would lead to substantially different spectra and fitted EXAFS parameters [54].

Table 1

Concentrations of (i) dissolved As, phosphate-extracted (PO₄) As, oxalate-extracted (Ox) As, and *aqua regia*-digested (AR) As; and (ii) oxalate-extracted (Ox) Fe and *aqua regia*-digested (AR) Fe in the dry sediment before the experiments (untreated sediment), in the control without ZVI (*t* = 30 d), and after treatment with ZVI at the end of phase A (23 d for nZVI/S-nZVI and 30 d for mZVI/S-mZVI). For comparison, expected “added” concentrations of ZVI are given (Nominal). Data are average values (± SD) for triplicate (AR) or duplicate analyses (PO₄ and Ox).

Treatment	As				Fe		Fe added		
	Dissolved	PO ₄	Ox	AR	Ox	AR	Ox ^b	AR ^a	Nominal
	mg/kg of dry sediment				g/kg of dry sediment		g/kg of dry sediment		
Control	4.6	7.3±0.3	27.8±1.3	41.7±1.1	0.69±0.01	7.3±0.5	-	-	-
mZVI	0.06	5.8±0.2	35.9±1.3	52.6±3.3	9.6±0.5	18.5±1.7	8.9	11.2	11.0
nZVI	0.11	5.6±0.0	37.0±3.3	51.4±2.5	3.0±0.2	9.8±0.4	2.3	2.5	3.1
S-mZVI	0.17	9.2±0.3	31.6±2.4	48.3±1.6	2.3±0.2	9.2±0.5	1.6	1.9	2.3
S-nZVI	0.67	8.4±0.0	34.8±1.5	48.0±0.9	2.9±0.1	10.7±1.2	2.2	3.4	3.3
Untreated	-	ND	37.6±0.1	53.9±5.2	0.65±0.02	8.7±2.0	-	-	-

^a Calculated as the difference between ZVI-treated samples and control. It represents the total amount of Fe(0) at the beginning (*t* = 0) of each ZVI treatment.

^b Calculated as the difference between ZVI-treated samples and control. It represents the amount of Fe(0) that turned into reactive Fe species at the end of phase A in each ZVI treatment.

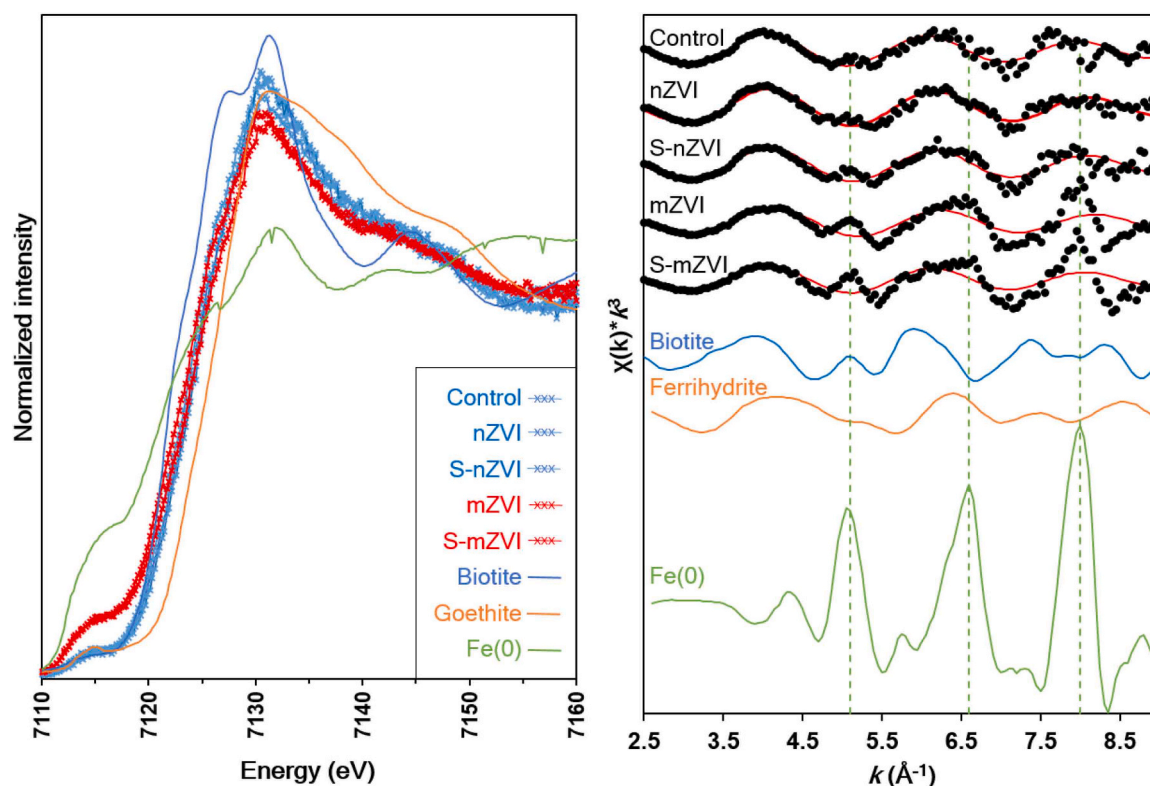


Fig. 4. (left) Normalized Fe K-edge XANES spectra for all samples at the end of phase A. For comparison, the XANES spectra of biotite, goethite, and Fe(0) foil are shown. (right) Fe K-edge k^3 -weighted EXAFS for samples (black dots) overlapped by model fits (red lines). For comparison, the EXAFS spectra of biotite, ferrihydrite, and Fe(0) foil are shown. The dashed vertical lines show the positions of features in the Fe(0) EXAFS data at 5.1, 6.6 and 8.0 \AA^{-1} .

Table 2

Fe speciation (percentage weights) at the end of phase A as evidenced from linear combination fitting with LCF-LinEst. The XANES spectra for the samples overlapped by the LCF fits are shown in Fig. S3.

Treatment	Fe(III) oxide ^a	Biotite	Fe(III)-org ^b	Fe(0)	NRSS ^c
Control	37.3 \pm 5.2	51.2 \pm 2.4	11.5 \pm 4.0	-	0.00044
mZVI	46.5 \pm 5.0	28.6 \pm 1.8	3.3 \pm 3.1	21.5 \pm 0.7	0.00015
S-mZVI	30.6 \pm 5.0	41.8 \pm 1.5	4.8 \pm 3.4	22.8 \pm 0.8	0.00030
nZVI	48.1 \pm 5.2	40.7 \pm 2.2	10.2 \pm 3.4	1.0 \pm 0.6	0.00029
S-nZVI	46.4 \pm 5.1	43.1 \pm 2.0	5.6 \pm 3.3	4.9 \pm 0.7	0.00032

^a Ferrihydrite or goethite;

^b Fe(III) complexed to fulvic acid;

^c Normalized residual sum-of-squares, see text

4. Discussion

4.1. Untreated sediment

The sediment core used for the experiments was taken from an area with confirmed anoxic groundwater ($E_h \sim 0$ mV) and high concentration of soluble As (200–2200 $\mu\text{g/L}$) (Table S8). Smedley and Kinniburgh [50] pointed out that many groundwaters around the world with high concentrations of As (> 1000 $\mu\text{g/L}$) frequently have fairly low concentration of solid-phase bound As (1–20 mg/kg) and proposed $E_h < 50$ mV as an indicator for groundwaters at risk for high dissolved As concentrations. Thus, geochemical conditions at the Hjaltevad site are typical for aquifers sensitive to As contamination.

XAS measurements indicated that As was mainly bound as As(V) to Fe/Al (hydr)oxides in the control with no ZVI addition (Section 3.3). However, a fraction of this pool was labile and solid-phase As(V) was reduced to mobile arsenite, resulting in high soluble concentrations of As (Fig. 1). Indeed, thermodynamic calculations revealed that

suspensions were close to the pH– E_h domain in which arsenite species could prevail in solution while arsenate species could prevail in the solid phase, considering the uncertainty in the E_h measurements (Fig. 6). For a constant pH, As reduction is expected to occur first in the solution phase followed by the solid phase as a response to lowering E_h , due to the stronger binding of arsenate compared to arsenite at $\text{pH} < \sim 9$. Measuring redox potential in weakly buffered solutions is notoriously difficult [11,15], which is apparent from the scattering of E_h data in Fig. 6. This was particularly true for solutions low in dissolved Fe(II), such as the control system and phase A solutions (no pH adjustment) in the mZVI, nZVI and S-nZVI treatments.

4.2. Uncoated ZVI materials

The two uncoated ZVI materials (mZVI and nZVI) were efficient in immobilizing As, resulting in solution As concentrations below 3 % of that in the control system. Arsenic in the ZVI-treated samples was dominated by As(V) species adsorbed to Fe and Al (hydr)oxides (Fig. 5). Dissolved As, though very low, was also dominated by As(V) species (Fig. 2). mZVI and nZVI addition thus appeared to promote the oxidation of soluble arsenite to As(V) species, driven by the increase in pH and largely in agreement with thermodynamic calculations (Fig. 6). Indeed, arsenite can be oxidized and bound as arsenate by Fe (hydr)oxides also under anoxic conditions [53,23]. Amstaetter et al. [2] reported rapid oxidation of arsenite to arsenate in Fe(II)-goethite systems under anoxic conditions, where Fe promoted electron transfer by forming a reactive Fe(III) intermediate phase with enhanced redox activity.

Most nZVI was transformed to Fe(III) (hydr)oxides during 23 days of reaction (Fig. 4, Table 2), consistent with the rapid oxidation kinetics of these nano-sized particles [58,67]. In contrast, about 1/3 of mZVI remained as Fe(0) after 30 days (Table 2), likely owing to their larger size and lower surface area that slow down oxidation. In both cases, the neoformed Fe (hydr)oxides were highly reactive as ca. 1/3 of the

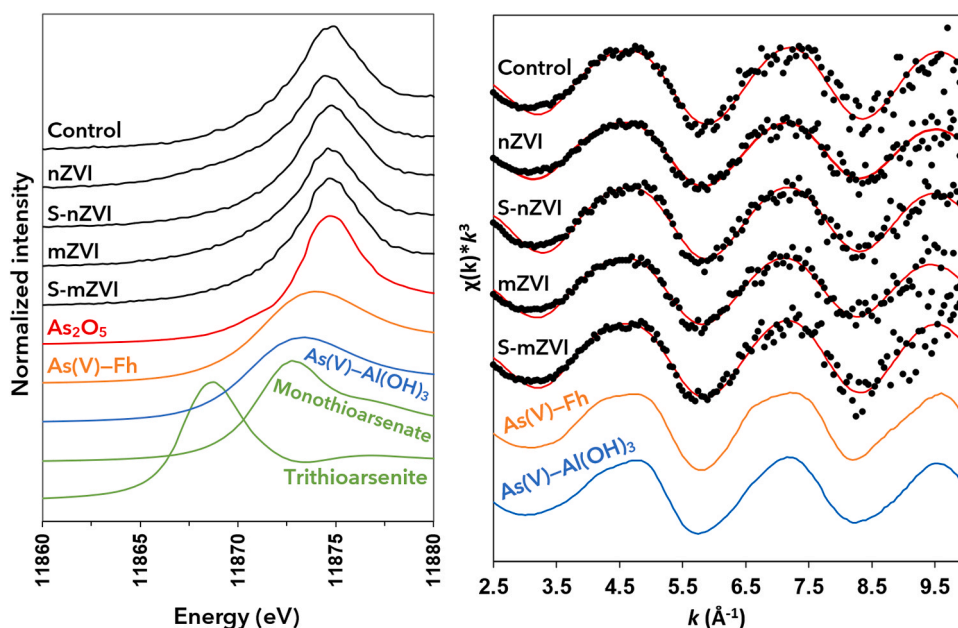


Fig. 5. (left) Normalized As K-edge XANES spectra for all samples at the end of phase A. For comparison, the XANES spectra of As(III) and As(V) reference compounds are shown. (right) As K-edge k^3 -weighted EXAFS. Sample data (black dots), model fits (red lines), and EXAFS data of AsO_4 adsorbed to ferrihydrite and AsO_4 adsorbed to $\text{Al}(\text{OH})_3$.

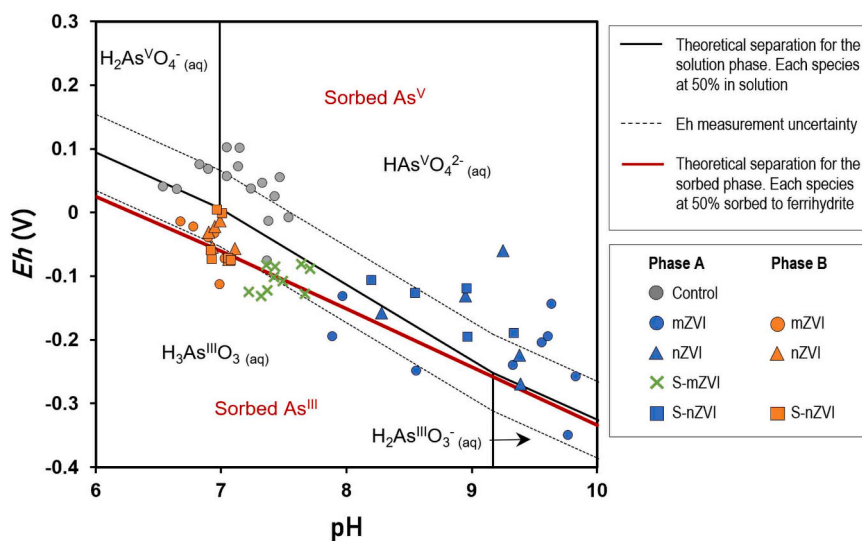


Fig. 6. Pourbaix diagram for the distribution of solution-phase (black lines) and sorbed-phase (red line, sorbed to ferrihydrite) As(III) and As(V) species together with pH x Eh points measured during equilibration of the control system and reaction with ZVI particles during phase A (uncontrolled pH) and phase B (pH 7). Input data and procedure for calculation are described in Tables S5, S6, and S7.

amount of Fe added as ZVI dissolved when the pH was adjusted to 7. In spite of that, As remained immobilized, which can be explained by the concomitant increase in Eh favoring the formation of arsenate that subsequently binds strongly to the remaining corrosion products (Fig. 6).

Our data could not confirm previous findings that As(III) can be reduced to either As(0) [28,58] or to an intermetallic phase (As-I) with Fe(0) [67] by nZVI at anoxic conditions. However, Mondal et al. [28] and Tuček et al. [58] used pyrophoric oxidic-shell-free nZVI particles (OSF-nZVI), which appears to favor the formation of As(0). In our experiment, we used freshly prepared suspensions of NANOFER 25 stored cool (+2–4 °C) for ca. one week, which naturally induces the formation of a thin iron oxide shell of a few nanometers [22]. This might explain the lack of As(0) formation in our experiment, although Yan

et al. [67] claimed that arsenite could diffuse across the oxide shell and subsequently be reduced by the Fe(0) core. Noteworthy, the studies cited above were conducted using aqueous suspensions of ZVI and added arsenite salts. Sediment material can compete with dissolved As for reaction with the ZVI materials and will also buffer the solution chemistry (e.g. pH and Eh) more compared to simple solutions due to solid-solution partitioning processes. In that respect, our study represents a more field realistic situation for an in situ treatment situation.

The potential long-term stability of immobilized As is a key issue for field applications of ZVI. In this respect, co-precipitation must be considered more favorable than surface complexation. Due to the relatively low concentration of As in our sample (53.9 mg/kg; Table 1), the K-edge As EXAFS spectra was of fairly poor quality, making a meaningful evaluation of second shell distances not possible (Fig. 5). Instead,

an indication of the “accessibility” of immobilized As was given by phosphate extractions. Assuming the labile pool of As is represented by the sum of dissolved As (during equilibration in phase A) and phosphate extractable As (after isolating the solid phase from the solution), a 50 % decrease in this pool was obtained using nZVI and mZVI (Table 1). This is in agreement with results obtained by Su and Puls [53], who found that the ability of phosphate to desorb As(III) and As(V) from ZVI decreased as the reaction time in dilute NaCl solutions increased from 1 to 60 days.

4.3. Sulfidated ZVI materials

The S-nZVI and nZVI tested in the present study were obtained from the same manufacturer, with S-nZVI prepared as a final coating to bare nZVI, allowing for a direct evaluation of the effect of sulfidation. Despite almost identical effects on pH and Eh, S-nZVI performed less well than its non-sulfidated counterpart, resulting in a ca. 10 times higher residual dissolved As concentration (Figs. 2 and 3). Even though some monothioarsenate formed using S-nZVI (Fig. 3, Table S2), this species had previously shown comparable removal rates than arsenate [34], which cannot explain the higher As solubility using S-nZVI observed here. XANES analysis showed that a major fraction of the Fe core of the S-nZVI particles was oxidized to Fe (hydr)oxides, similarly to the non-sulfidated nZVI (Table 2). However, SO_4^{2-} concentrations in solution did not increase compared to control systems (Fig. S4) and dissolved sulfide was close to the detection limit (0.01 mg/L; Table S2), indicating that the Fe-S surface layer remained mostly insoluble during the experimental period. This suggests that the FeS coating remained on the surface of the oxidized Fe core in a way that impaired As immobilization.

Our data do not support previous studies made with anoxic aqueous suspensions of sulfidated and uncoated ZVI materials, showing a superior immobilization capacity for sulfidated ZVI. Wu et al. [66] found an optimal As removal capacity at S/Fe molar ratio of 0.2, whereas Singh et al. [45] and Zhao et al. [68] observed an optimal removal capacity at S/Fe molar ratio of 0.1. The increased efficiency was assigned to additional removal mechanism(s) involving As-S precipitation [45,66,68]. One possible explanation for the discrepancy between the results obtained in these studies and here is that previous investigations used simple aqueous suspensions consisting only of ZVI particles and added arsenite salts whereas here complex groundwater conditions were simulated by using a field As-contaminated sediment. In spite of the anoxic conditions verified during the experimental period, addition of S-nZVI particles to our sediment suspensions favored arsenate in the solution phase (Fig. 3, Table S2), impairing formation of any As(III)-S precipitates. This explains the low rate of thiolation, since arsenite is required as precursor for thiolation [4].

A comparison between micro-sized mZVI and S-mZVI also indicated that sulfidation hindered immobilization of As (Figs. 2 and 3). However, the results are not directly comparable since the dose of mZVI was five times higher than that of S-mZVI. On the other hand, the dose of S-mZVI and S-nZVI particles was the same, showing a better performance for the S-mZVI material compared to S-nZVI. This is opposite to what could be expected based on the surface areas of the two materials, but can be explained by the lower pH obtained in the S-mZVI system compared to the S-nZVI system, favoring the immobilization of As(V) by the Fe(III) corrosion products formed. The fact that only a minor fraction of the Fe (0) core was oxidized in the S-mZVI system (Table 2, Fig. 4) could be favorable in a long-term perspective in field applications.

For all four studied ZVIs, the sorption mechanism seems to be the same, i.e. oxidation of solution arsenite to arsenate followed by sorption of arsenate to the Fe(III) (hydr)oxide corrosion product(s) formed. This process is partly driven by the increase in pH caused by oxidation of the ZVI core (Reaction 1), which favors the stability of arsenate relative to that of arsenite (Fig. 6). However, the slow Fe(0) oxidation in the S-mZVI system suggests that ZVI particles themselves also contributed to the oxidation of arsenite. Despite the similar pH in the control and S-

mZVI systems (ca. 7.5), with redox potential even somewhat lower in the S-mZVI system, soluble As was strongly dominated by arsenate in S-mZVI treated sediments (Fig. 3, Table S2), whereas arsenite dominated in the control system (Fig. 1). The exact mechanism is unclear, but the simultaneous existence of an Fe(III) (hydr)oxide phase and dissolved Fe (II) could possibly facilitate the oxidation of arsenite to arsenate, as indicated by the results of Amstetter et al. [2].

5. Conclusions

All experiments were performed using sediment material sampled from a historically As-contaminated aquifer, with focus on investigating the potential ability of different ZVI materials to immobilize As in situ, thus preventing further spread of As from the source zone. Batch experiments performed without ZVI addition showed that arsenite dominated in solution, in accordance with prior field measurements of As speciation in the groundwater at the site. The chemical conditions observed both in laboratory experiments and in field measurements were typical for aquifers sensitive to As contamination, i.e. pH ~7 and Eh < 50 mV, suggesting a broad relevance of the results obtained in the present study for field situations.

Uncoated ZVI materials, both in nano- and microscale, performed better than their sulfidated counterparts, highlighting the important role of corrosion products (Fe(III) (hydr)oxides) in binding As. Solution and solid-phase speciation of As suggested that arsenite was oxidized and subsequently immobilized by Fe(0) corrosion products in all ZVI materials. In addition, phosphate extractions indicated that As(V) immobilization by uncoated nZVI and mZVI particles, at least partly, was due to occlusion of As by Fe(III) (hydr)oxide corrosion products. Non-sulfidated ZVI materials are thus promising in situ agents for long-term immobilization of As.

In a long-term perspective, the particle size (micro vs. nano) of the ZVI sorbents probably will have a fairly small effect on their As immobilization capacity, since nano-sized nZVI and S-nZVI did not perform better than their micro-sized counterparts mZVI and S-mZVI (Figs. 2 and 3). This is likely because immobilization was related to corrosion products formed, rather than the initial size of the particles. Hence, the ZVI dose will have a larger impact on the As immobilization performance. Our results provide a strong geochemical background for the application of ZVI particles to remove As from anoxic contaminated groundwaters.

CRedit authorship contribution statement

Thiago Augusto Formentini: Conceptualization, Methodology, Formal analysis, Investigation, Writing – Original Draft. **Geert Cornelis:** Conceptualization, Methodology, Formal analysis, Investigation, Resources, Writing - Review & Editing, Funding acquisition. **Jon Petter Gustafsson:** Conceptualization, Methodology, Formal analysis, Investigation, Resources, Writing - Review & Editing, Funding acquisition. **Kathrin Leicht:** Investigation, Formal analysis. **Charlotta Tiberg:** Formal analysis, Validation, Writing - Review & Editing. **Britta Planer-Friedrich:** Methodology, Validation, Resources, Writing - Review & Editing. **Neal Durant:** Validation, Writing - Review & Editing. **Dimin Fan:** Validation, Writing - Review & Editing. **Dan B. Kleja:** Conceptualization, Methodology, Formal analysis, Resources, Writing - Review & Editing, Supervision, Project administration, Funding acquisition.

Declaration of Competing Interest

The authors declare that they have no known competing financial interests or personal relationships that could have appeared to influence the work reported in this paper.

Data availability

Data will be made available on request.

Acknowledgements

The research was funded by the Swedish Geotechnical Institute (SGI)'s research program Tuffo, under contract 1.1–1905-0340 and Telia Company. We acknowledge MAX IV Laboratory for time on beamline Balder under proposals 20190720 and 20200265. Research conducted at MAX IV, a Swedish national user facility, is supported by the Swedish Research council under contract 2018–07152, the Swedish Governmental Agency for Innovation Systems under contract 2018–04969, and Formas under contract 2019–02496. The authors are grateful to Susan Nehzati for excellent help during the beamtime, Mina Spångberg for laboratory support, Per Persson and Dean Hesterberg for kindly providing some of the standards for Fe K-edge XAS, and to Steve Hillier for providing high-quality X-Ray Powder Diffraction data of the untreated Hjärtevad sample. Finally, the authors acknowledge Pär Hallgren (SWECO), for performing the sediment sampling at Hjärtevad. Abstract art created with BioRender.

Appendix A. Supporting information

Supplementary data associated with this article can be found in the online version at [doi:10.1016/j.jhazmat.2023.132743](https://doi.org/10.1016/j.jhazmat.2023.132743).

References

- Almkvist, G., Boye, K., Persson, I., 2010. K-edge XANES analysis of sulfur compounds: an investigation of the relative intensities using internal calibration. *J Synchrotron Radiat* 17, 683–688. <https://doi.org/10.1107/S0909049510022946>.
- Amstaetter, K., Borch, T., Larese-Casanova, P., Kappler, A., 2010. Redox transformation of arsenic by Fe(II)-activated goethite (α -FeOOH). *Environ Sci Technol* 44 (1), 102–108. <https://doi.org/10.1021/es901274s>.
- Belluck, D.A., Benjamin, S.L., Baveye, P., Sampson, J., Johnson, B., 2003. Widespread arsenic contamination of soils in residential areas and public spaces: an emerging regulatory or medical crisis. *Int J Toxicol* 22 (2), 109–128. <https://doi.org/10.1080/10915810305087>.
- Besold, J., Biswas, A., Suess, E., Scheinost, A.C., Rossberg, A., Mikutta, C., Kretzschmar, R., Gustafsson, J.P., Planer-Friedrich, B., 2018. Monothioarsenate transformation kinetics determining arsenic sequestration by sulfhydryl groups of peat. *Environ Sci Technol* 52 (13), 7317–7326.
- Brumovský, M., Filip, J., Malina, O., Oborná, J., Sracek, O., Reichenauer, T.G., Andrášková, P., Zboril, R., 2020. Core-shell Fe/FeS nanoparticles with controlled shell thickness for enhanced trichloroethylene removal. *ACS Appl Mater Interfaces* 12 (31), 35424–35434. <https://doi.org/10.1021/acsami.0c08626>.
- Brumovský, M., Oborná, J., Lacina, P., Hegedüs, M., Sracek, O., Kolarík, J., Petr, M., Kašík, J., Hofmann, T., Filip, J., 2021. Sulfidated nano-scale zerovalent iron is able to effectively reduce in situ hexavalent chromium in a contaminated aquifer. *J Hazard Mater* 405, 124665. <https://doi.org/10.1016/j.jhazmat.2020.124665>.
- Cao, F., Kleja, D.B., Tibergh, C., Jarsjö, J., 2023. Large-scale arsenic mobilization from legacy sources in anoxic aquifers: Multiple methods and multi-decadal perspectives. *Sci Total Environ* 892, 164565. <https://doi.org/10.1016/j.scitotenv.2023.164565>.
- Couture, R.-M., Rose, J., Kumar, N., Mitchell, K., Wallschläger, D., Van Cappellen, P., 2013. Sorption of arsenite, arsenate, and thioarsenates to iron oxides and iron sulfides: a kinetic and spectroscopic investigation. *Environ Sci Technol* 47 (11), 5652–5659. <https://doi.org/10.1021/es3049724>.
- D'Angelo, P., Benfatto, M., 2004. Effect of multielectronic configurations on the XAFS Analysis at the Fe K edge. *J Phys Chem A* 108 (20), 4505–4514. <https://doi.org/10.1021/jp0499732>.
- Fan, D., Lan, Y., Tratnyek, P.G., Johnson, R.L., Filip, J., O'Carroll, D.M., Nunez Garcia, A., Agrawal, A., 2017. Sulfidation of iron-based materials: a review of processes and implications for water treatment and remediation. *Environ Sci Technol* 51 (22), 13070–13085. <https://doi.org/10.1021/acs.est.7b04177>.
- Gezahegne, W.A., Planer-Friedrich, B., Merkel, B.J., 2007. Obtaining stable redox potential readings in gneiss groundwater and mine water: difficulties, meaningfulness, and potential improvement. *Hydrogeol J* 15 (6), 1221–1229. <https://doi.org/10.1007/s10040-007-0174-0>.
- Gustafsson, J.P. (2013). Visual MINTEQ 3.1. (<http://vminteq.lwr.kth.se/>).
- Gustafsson, J.P. (2022). LCF-LinEst. Web: (<https://vminteq.com/lcf-linest/>).
- Gustafsson, J.P., Braun, S., Tuyishime, J.R.M., Adediran, G.A., Warrinner, R., Hesterberg, D., 2020. A probabilistic approach to phosphorus speciation of soils using P K-edge XANES spectroscopy with linear combination fitting. *Soil Syst* 4, 26. <https://doi.org/10.3390/soilsystems4020026>.
- Holm, T.R., Curtiss, C.D., 1989. A comparison of oxidation-reduction potentials calculated from the As(V)/As(III) and Fe(III)/Fe(II) couples with measured platinum-electrode potentials in groundwater. *J Contam Hydrol* 5 (1), 67–81. [https://doi.org/10.1016/0169-7722\(89\)90006-5](https://doi.org/10.1016/0169-7722(89)90006-5).
- Hopp, L., Peiffer, S., Durner, W., 2006. Spatial variability of arsenic and chromium in the soil water at a former wood preserving site. *J Contam Hydrol* 85, 159–178. <https://doi.org/10.1016/j.jconhyd.2006.01.005>.
- ISO 11466, "Soil Quality, Extraction of Trace Elements Soluble in Aqua Regia," International Organization for Standardization, 1995.
- Kelly, S.D., Hesterberg, D., Ravel, B., 2008. Analysis of soils and minerals using X-ray absorption spectroscopy. *Soil Science of America Book series No. 5*. In: Ulery, A.L., Drees, L.R. (Eds.), *Methods of Soils Analysis. Part 5. Mineralogical Methods*. Soil Science of America, Madison, WI, pp. 387–463. <https://doi.org/10.2136/sssabookser5.5.c14>.
- Kirk, M.F., Roden, E.E., Crossey, L.J., Brearley, A.J., Spilde, M.N., 2010. Experimental analysis of arsenic precipitation during microbial sulfate and iron reduction in model aquifer sediment reactors. *Geochim Et Cosmochim Acta* 74 (9), 2538–2555. <https://doi.org/10.1016/j.gca.2010.02.002>.
- Kitahama, K., Kiriya, R., Baba, Y., 1975. Refinement of the crystal structure of scorodite. *Acta Crystallogr B* 31, 322–324. <https://doi.org/10.1107/S056774087500266X>.
- Lipczynska-Kochany, E., Harms, S., Milburn, R., Sprah, G., Nadarajah, N., 1994. Degradation of carbon tetrachloride in the presence of iron and sulphur containing compounds. *Chemosphere* 29 (7), 1477–1489. [https://doi.org/10.1016/0045-6535\(94\)90279-8](https://doi.org/10.1016/0045-6535(94)90279-8).
- Liu, A., Zhang, W.X., 2014. Fine structural features of nanoscale zero-valent iron characterized by spherical aberration corrected scanning transmission electron microscopy (Cs-STEM). *Analyst* 139 (18), 4512–4518. <https://doi.org/10.1039/c4an00679h>.
- Manning, B.A., Hunt, M.L., Amrhein, C., Yarmoff, J.A., 2002. Arsenic(III) and Arsenic(V) Reactions with Zerovalent Iron Corrosion Products. *Environ. Sci. Technol.* 36, 5455–5461. <https://doi.org/10.1021/es0206846>.
- Meng, X., Korfiatis, G.P., Jing, C., Christodoulatos, C., 2001. Redox transformations of arsenic and iron in water treatment sludge during aging and TCLP extraction. *Environ Sci Technol* 35, 3476–3481. <https://doi.org/10.1021/es010645e>.
- Michel, F.M., Ehm, L., Antao, S.M., Lee, P.L., Chupas, P.J., Liu, G., Strongin, D.R., Schoonen, M.A.A., Phillips, B.L., Parise, J.B., 2007. The Structure of Ferrihydrite, a Nanocrystalline Material. *Science* 316 (5832), 1726–1729. <https://doi.org/10.1126/science.114252>.
- Mikutta, C., 2011. X-ray absorption spectroscopy study on the effect of hydroxybenzoic acids on the formation and structure of ferrihydrite. *Geochim Et Cosmochim Acta* 75, 5122–5139. <https://doi.org/10.1016/j.gca.2011.06.002>.
- Mikutta, C., Mandaliev, P.N., Kretzschmar, R., 2013. New clues to the local atomic structure of short-range ordered ferric arsenate from extended X-ray absorption fine structure spectroscopy. *Environ Sci Technol* 47, 3122–3131. <https://doi.org/10.1021/es3051795>.
- Mondal, P., Bhowmick, S., Jullo, N., Ye, W., Van Renterghem, W., Van Den Bergh, S., Van Der Bruggen, B., 2014. Behavior of As(V) with ZVI-H₂O system and the reduction to As(0). *J Phys Chem C* 118 (37), 21614–21621. <https://doi.org/10.1021/jp505174k>.
- Morais, S., Fonseca, H.M.A.C., Oliveira, S.M.R., Oliveira, H., Gupta, V.K., Sharma, B., de Lourdes Pereira, M., 2021. Environmental and health hazards of chromated copper arsenate-treated wood: a review. *Int J Environ Res Public Health* 18, 5518. <https://doi.org/10.3390/ijerph18115518>.
- Morris, A.J., Hesterberg, D.L., 2012. Iron(III) coordination and phosphate sorption in peat reacted with ferric or ferrous iron. *Soil Sci Soc Am J* 76, 101–109. <https://doi.org/10.2136/sssaj2011.0097>.
- Nriagu, J.O., Bhattacharya, P., Mukherjee, A.B., Bundschuh, J., Zevenhoven, R., Loeppert, R.H., 2007. Arsenic in soil and groundwater: an overview. *Trace Met Other Contam Environ* 9, 3–60. [https://doi.org/10.1016/S1875-1121\(06\)09001-8](https://doi.org/10.1016/S1875-1121(06)09001-8).
- O'Carroll, D., Sleep, B., Krol, M., Boparai, H., Kocur, C., 2013. Nanoscale zero valent iron and bimetallic particles for contaminated site remediation. *Adv Water Resour* 51, 104–122. <https://doi.org/10.1016/j.advwatres.2012.02.005>.
- Parfitt, R.L., Childs, C.W., 1988. Estimations of forms of Fe and Al – a review, and analysis of contrasting soils by dissolution and Mossbauer methods. *Aust J Soil Res* 26 (1), 121–144. <https://doi.org/10.1071/SR9880121>.
- Planer-Friedrich, B., Schaller, J., Wismeth, F., Mehlhorn, J., Hug, S.J., 2018. Monothioarsenate occurrence in bangladesh groundwater and its removal by ferrous and zero-valent iron technologies. *Environ Sci Technol* 52 (10), 5931–5939.
- Polya, D.A., Middleton, D.R.S., 2017. Arsenic in drinking water: sources & human exposure. *Best Practice Guide on the Control of Arsenic in Drinking Water*. IWA Publishing, pp. 1–24. <https://doi.org/10.2166/9781780404929.001>.
- Prietz, J., Thieme, J., Eusterheus, K., Eichert, D., 2007. Iron speciation in soils and soil aggregates by synchrotron-based X-ray microspectroscopy (XANES, μ -XANES). *Eur J Soil Sci* 58, 1027–1041. <https://doi.org/10.1111/j.1365-2389.2006.00882.x>.
- Ramos, M.A., Yan, W., Li, X., Koel, B.E., Zhang, W., 2009. Simultaneous oxidation and reduction of arsenic by zero-valent iron nanoparticles: understanding the significance of the core-shell structure. *J Phys Chem C* 113 (33), 14591–14594. <https://doi.org/10.1021/jp9051837>.
- Ravel, B., Newville, M., 2005. Athena, Artemis, Hephaestus: data analysis for X-ray absorption spectroscopy using IFFEFIT. *J Synchrotron Radiat* 12, 537–541. <https://doi.org/10.1107/S0909049505012719>.

- [39] Rehr, J.J., Kas, J.J., Prange, M.P., Sorini, A.P., Takimoto, Y., Vila, F., 2009. Ab initio theory and calculations of X-ray spectra. *Comptes Rendus Phys* 10 (6), 548–559. <https://doi.org/10.1016/j.crhy.2008.08.004>.
- [40] Saxe, J.K., Wannamaker, E.J., Conklin, S.W., Shupe, T.F., Beck, B.D., 2007. Evaluating landfill disposal of chromated copper arsenate (CCA) treated wood and potential effects on groundwater: Evidence from Florida. *Chemosphere* 66, 496–504. <https://doi.org/10.1016/j.chemosphere.2006.05.063>.
- [41] Schmid, D., Micić, V., Laumann, S., Hofmann, T., 2015. Measuring the reactivity of commercially available zero-valent iron nanoparticles used for environmental remediation with iopromide. *J Contam Hydrol* 181, 36–45. <https://doi.org/10.1016/j.jconhyd.2015.01.006>.
- [42] Serjeant, E.P., & Dempsey, B. (1979). Ionisation constants of organic acids in aqueous solution. IUPAC chemical data series, 23. New York, NY: Pergamon, 989 p.
- [43] Shaji, E., Santosh, M., Sarath, K. v., Prakash, P., Deepchand, V., Divya, B., 2021. Arsenic contamination of groundwater: a global synopsis with focus on the Indian Peninsula. *Geosci Front* 12 (3), 101079. <https://doi.org/10.1016/j.gsf.2020.08.015>.
- [44] Shi, Z., Fan, D., Johnson, R.L., Tratnyek, P.G., Nurmi, J.T., Wu, Y., Williams, K.H., 2015. Methods for characterizing the fate and effects of nano zerovalent iron during groundwater remediation. *J Contam Hydrol* 181, 17–35. <https://doi.org/10.1016/j.jconhyd.2015.03.004>.
- [45] Singh, P., Pal, P., Mondal, P., Saravanan, G., Nagababu, P., Majumdar, S., Labhsetwar, N., Bhowmick, S., 2021. Kinetics and mechanism of arsenic removal using sulfide-modified nanoscale zerovalent iron. *Chem Eng J* 412, 128667, 1016/j.cej.2021.128667.
- [46] SIS – Swedish institute for standards. (1997). SS-EN 1484. Water analysis - Guidelines for the determination of total organic carbon (TOC) and dissolved organic carbon (DOC). Stockholm, 1st edition, 21 p.
- [47] SIS – Swedish institute for standards. (2009). SS-EN ISO 10304–1:2009. Water quality - Determination of dissolved anions by liquid chromatography of ions - Part 1: Determination of bromide, chloride, fluoride, nitrate, nitrite, phosphate and sulfate. Stockholm, 2nd edition, 28 p.
- [48] SIS – Swedish institute for standards. (2016). SS-EN ISO 17294–2:2016. Water quality - Application of inductively coupled plasma mass spectrometry (ICP-MS) - Part 2: Determination of selected elements including uranium isotopes. Stockholm, 2nd edition, 44 p.
- [49] SIS – Swedish institute for standards. (2018). SS-EN ISO 15681–2:2018. Water quality - Determination of orthophosphate and total phosphorus contents by flow analysis (FIA and CFA) - Part 2: Method by continuous flow analysis (CFA). Stockholm, 2nd edition, 32 p.
- [50] Smedley, P.L., Kinniburgh, D.G., 2002. A review of the source, behaviour and distribution of arsenic in natural waters. *Appl Geochem* 17 (5), 517–568. [https://doi.org/10.1016/S0883-2927\(02\)00018-5](https://doi.org/10.1016/S0883-2927(02)00018-5).
- [51] Smedley, P.L., Kinniburgh, D.G., 2013. Arsenic in groundwater and the environment. In: Selinus, O. (Ed.), *Essentials of Medical Geology: Revised Edition*. Springer, Netherlands, Dordrecht, pp. 279–310. https://doi.org/10.1007/978-94-007-4375-5_12.
- [52] Smedley, P.L., Zhang, M., Zhang, G., Luo, Z., 2001. Arsenic and other redox-sensitive elements in groundwater from the Huhhot Basin, Inner Mongolia. In: Cidu, R. (Ed.), *Water-Rock Interaction*, 10. Taylor and Francis, pp. 181–184.
- [53] Su, C., Puls, R.W., 2001. Arsenate and arsenite removal by zerovalent iron: effects of phosphate, silicate, carbonate, borate, sulfate, chromate, molybdate, and nitrate, relative to chloride. *Environ Sci Technol* 35 (22), 4562–4568. <https://doi.org/10.1021/es010768z>.
- [54] Suess, E., Scheinost, A.C., Bostick, B.C., Merkel, B.J., Wallschlaeger, D., Planer-Friedrich, B., 2009. Discrimination of thioarsenites and thioarsenates by X-ray absorption spectroscopy. *Environ Sci Technol* 43 (12), 8318–8326. <https://doi.org/10.1021/ac901094b>.
- [55] Sundman, A., Karlsson, T., Laudon, H., Persson, P., 2014. XAS study of iron speciation in soils and waters from a boreal catchment. *Chem Geol* 364, 93–102. <https://doi.org/10.1016/j.chemgeo.2013.11.023>.
- [56] Thompson, A., Attwood, D., Gullikson, E., Howells, M., Kim, K.J., Kirz, J., Kortright, J., Lindau, I., Pianetta, P., Robinson, A., Scofield, J., Underwood, J., Williams, G., Winck, H., 2009. X-ray Data Booklet. Lawrence Berkeley National Laboratory. University of California, Berkeley, California.
- [57] Tosco, T., Petrangeli Papini, M., Cruz Viggi, C., Sethi, R., 2014. Nanoscale zerovalent iron particles for groundwater remediation: a review. *J Clean Prod* 77, 10–21. <https://doi.org/10.1016/j.jclepro.2013.12.026>.
- [58] Tuček, J., Pucek, R., Kolařík, J., Zoppellaro, G., Petr, M., Filip, J., Sharma, V.K., Zbořil, R., 2017. Zero-valent iron nanoparticles reduce arsenites and arsenates to As(0) firmly embedded in core-shell superstructure: challenging strategy of arsenic treatment under anoxic conditions. *ACS Sustain Chem Eng* 5 (4), 3027–3038. <https://doi.org/10.1021/acssuschemeng.6b02698>.
- [59] U.S. EPA. 1994. "Method 200.8: Determination of Trace Elements in Waters and Wastes by Inductively Coupled Plasma-Mass Spectrometry," Revision 5.4. Cincinnati, OH.
- [60] van Reeuwijk, L.P. (2002). Procedures for soil analysis (6th edition). Technical Paper No. 9, ISRIC, Wageningen.
- [61] van Schaik, J.W.J., Persson, I., Kleja, D.B., Gustafsson, J.P., 2008. EXAFS study on the reactions between iron and fulvic acid in acid aqueous solutions. *Environ Sci Technol* 42, 2367–2373. <https://doi.org/10.1021/es072092z>.
- [62] Vega, A.S., Planer-Friedrich, B., Pastén, P.A., 2017. Arsenite and arsenate immobilization by preformed and concurrently formed disordered mackinawite (FeS). *Chem Geol* 475, 62–75. <https://doi.org/10.1016/j.chemgeo.2017.10.032>.
- [63] Wang, J., Kerl, C.F., Hu, P., Martin, M., Mu, T., Brüggewirth, L., Wu, G., Said-Pullichino, D., Romani, M., Wu, L., Planer-Friedrich, B., 2020. Thiolated arsenic species observed in rice paddy pore waters. *Nat Geosci* 13 (4), 282–287. <https://doi.org/10.1038/s41561-020-0533-1>.
- [64] Wenzel, W.W., Kirchbaumer, N., Prohaska, T., Stingeder, G., Lombi, E., Adriano, D. C., 2001. Arsenic fractionation in soils using an improved sequential extraction procedure. *Anal Chim Acta* 436, 309–323. [https://doi.org/10.1016/S0003-2670\(01\)00924-2](https://doi.org/10.1016/S0003-2670(01)00924-2).
- [65] Wolthers, M., Charlet, L., Van der Weijden, C.H., Van der Linde, P.R., Rickard, D., 2005. Arsenic mobility in the ambient sulfidic environment: sorption of arsenic(V) and arsenic(III) onto disordered mackinawite. *Geochim Et Cosmochim Acta* 69 (14), 3483–3492. <https://doi.org/10.1016/j.gca.2005.03.003>.
- [66] Wu, D., Peng, S., Yan, K., Shao, B., Feng, Y., Zhang, Y., 2018. Enhanced As(III) sequestration using sulfide-modified nano-scale zero-valent iron with a characteristic core-shell structure: sulfidation and as distribution. *ACS Sustain Chem Eng* 6 (3), 3039–3048. <https://doi.org/10.1021/acssuschemeng.7b02787>.
- [67] Yan, W., Vasic, R., Frenkel, A.I., Koel, B.E., 2012. Intraparticle reduction of arsenite (As(III)) by nanoscale zerovalent iron (nZVI) investigated with in situ X-ray absorption spectroscopy. *Environ Sci Technol* 46 (13), 7018–7026. <https://doi.org/10.1021/es2039695>.
- [68] Zhao, J., Su, A., Tian, P., Tang, X., Collins, R.N., He, F., 2021. Arsenic (III) removal by mechanochemically sulfidated microscale zero valent iron under anoxic and oxic conditions. *Water Res* 198, 117132. <https://doi.org/10.1016/j.watres.2021.117132>.